

Article

CO₂ Adsorption–Desorption Kinetics from the Plane Sheet of Hard Coal and Associated Shrinkage of the Material

Norbert Skoczylas¹, Anna Pajdak¹ and Mariusz Młynarczuk^{2,*} 

¹ The Strata Mechanics Research Institute of the Polish Academy of Sciences, Reymonta 27, 30-059 Cracow, Poland; skoczylas@imgpan.pl (N.S.); pajdak@imgpan.pl (A.P.)

² Faculty of Geology, Geophysics and Environmental Protection, AGH University of Science and Technology, Mickiewicza 30, 30-059 Cracow, Poland

* Correspondence: mlynar@agh.edu.pl; Tel.: +48-12-617-4864

Received: 9 September 2019; Accepted: 18 October 2019; Published: 22 October 2019



Abstract: The paper presents the results of studies on sorption and CO₂ desorptions from coals from two Polish mines that differed in petrographic and structural properties. The tests were carried out on spherical and plane sheet samples. On the basis of the sorption tests, the effective diffusion coefficient was calculated on the plane sheet samples based on a proper model. Similar tests were performed on the spherical samples. Mathematical model results for plane sheet samples were compared with the most frequently chosen model for spherical samples. The kinetics of CO₂ desorption from plane sheet samples were compared with the kinetics of sample shrinkage. In both samples, the shrinkage was about 0.35%. The size change kinetics and CO₂ desorption kinetics significantly differed between the samples. In both samples, the determined shrinkage kinetics was clearly faster than CO₂ kinetics.

Keywords: coal structure; coal petrography; swelling/shrinking of coal matrix; diffusion model of plane sheet; sorption/desorption of CO₂

1. Introduction

From a geological point of view, coal is a highly heterogeneous rock and a collector for gases naturally occurring in coal seams and fluids. Natural deposits of coal are characterized by a network of fissures and cracks as well as pores of various diameters. Depending on geological factors, including tectonic stress and near-fault areas, the crack network may occur with varying intensity [1,2]. The pores in coal comprise macropores with diameters above 50 nm, mesopores (2–50 nm) and micropores with diameters below 2 nm [3]. In the category of micro-pores, Sing et al. [4] distinguished additionally ultra-micropores with diameters not exceeding 0.8 nm. According to the literature [5–7] 90% of the pore space in coal consists of pores with a diameter below 1 nm. Therefore, coal is mainly treated as an ultra-microporous material. An extensive network of pores in coal affects the values of their structural parameters. The authors [8–11] analyzes the structure of coals by volumetric method in the pressure range of 0–0.1 MPa with N₂ (77 K) and CO₂ (273 K) as adsorbates. In [8–10] the measured coals differed in maceral composition. In the measurement using N₂, a sample with the highest content of vitrinite and low reflectance noted the total pore volume at the level of 26.6 mm³/g and the specific surface area (SSA) of 15.40 m²/g, based on the Brunauer, Emmett and Teller model (BET). In the other samples that contained less vitrinite, the pore volumes were much lower (from 1.7 to 1.9 mm³/g) and the SSA was in the range of 0.31–0.55 m²/g. In the measurement using CO₂, the values of those parameters were higher and the highest were found in coal of the lowest reflectance. The pore volumes were in the range of 23.8–39.7 mm³/g and the SSA from 87.9 to 138.2 m²/g. At work Okolo et al. [11] using N₂, a pore volume at the level of 1.01–1.47 mm³/g and a SSA (BET) of 2.6–5.7 m²/g was obtained. Using a

CO₂ adsorbate, a pore volume at the level of 4.3–5.2 mm³/g and a SSA of 107–129 m²/g was obtained, based on the Dubinin-Raduszkiewicz model (DR). Weishauptová and Sýkorová [12] studied the carbon structure by gravimetry method, at 0–0.1 MPa and they used CO₂ as the adsorbate at 298 K. They used the Langmuir model and obtained a pore volume of 11.6–17.7 cm³/g and a SSA of 83–120 m²/g.

Ultra-micropores in coal also have high sorption capacity, which depends, among others on the maceral and mineral composition of coal and its physical parameters [13–15]. Coal sorption capacity is affected by, among others functional groups, carbon metamorphism, maceral and mineral composition, as well as physical parameters [15,16]. The maceral composition of coal is important in the assessment of coal structure and sorption processes. Their classification can be performed by optical methods or automatically using artificial intelligence (AI) methods [14]. Coals with a high content of vitrinite macerals have a higher sorption capacity. In coals with a high content of inertinite maceral, the values of sorption parameters are much lower. In Pajdak et al. [17], the authors examines the competitive sorption of methane and carbon dioxide sorption under 0–1.0 MPa. The sorption capacity on coals, determined by gravimetric method, was for pure CH₄ at the level 0.31 mmolCH₄/g and for pure CO₂—0.65 mmolCO₂/g.

Among the pores, the ultra-micropores are comparable in size to gas adsorbate particles and exhibit flexibility that is responsible for matrix swelling/shrinkage. Coal matrix deformation processes as a result of gas desorption/adsorption are obvious, although not well explored. There are theoretical models and experimental works describing the swelling/shrinkage process in coal. Pan and Connell [18] created a theoretical model describing adsorption-induced coal swelling, where the change in surface energy caused by adsorption is equal to the change in energy of the flexible body of coal. Liu and Harpalani [19] developed a model of coal volume changes, which is based on the theory of surface energy changes as a result of sorption, while Connell et al. [20] determined the impact of coal deformation on its porosity. Durucan et al. [21] studied the deformability of coals with varying levels of carbonization under the influence of CO₂ and CH₄ sorption.

The processes of swelling and shrinking of the coal matrix have different origin. The shrinking of the coal matrix occurs during the primary formation of methane, which triggers phenomena related to the reduction of effective horizontal stress. Due to the pressure drop, the reservoir compaction occurs, which increases the effective horizontal stress. Another phenomenon is the desorption of gas from the coal matrix, which reduces the horizontal stress and, as a result, shrinks the coal matrix.

Swelling of the coal matrix occurs during CO₂ storage in coal or ECBM technology. Due to the fact that the sorption affinity of coal to CO₂ is higher than to CH₄, the CO₂ adsorption results in swelling of the coal matrix. The values of swelling and shrinkage of the coal matrix caused by CO₂ adsorption and desorption are usually 1.5–5 times higher than the values of the same processes in the presence of CH₄ [21,22].

Desorption of gas sorbate from heterogeneous materials, including coal, comprises several processes. The gas molecule that leaves the coal structure is desorbed in the first stage. Desorption understood as an increase in the number of degrees of freedom of gas molecules is an almost instantaneous process [23]. Desorption initiates gas transport in a complex pore structure of coal. Traditionally, transport on a single-grain scale, treated as a monolithic area not cut by a crack network, is described as diffusion that is a combination of a number of mechanisms [24–28]. Molecular diffusion occurs when the average free path of gas molecules is significantly smaller than the pore size [29]. Knudsen diffusion occurs when the average free path of gas molecules is greater than the pore size. Collisions of gas molecules with pore walls play an important role. Volmer surface diffusion occurs when there is a concentration gradient of adsorbed gas molecules along the surface of a solid. Gas migration along the solid surface is possible thanks to the energetic heterogeneity of the surface. Diffusion in extremely narrow pores (solid diffusion) comparable to the size of gas molecules (diffusion in a solid body) applies when the pore diameter is close to the diameter of the gas molecules. A gas molecule permeating such small pores must have sufficient energy for it to be transported. It is called activated diffusion. The thermal vibrations of the sorbent network are conducive to this process.

It follows from the research [30–32] that coal swelling that results from sorption also exhibits a kinetic feature: coal swelling increases over time until swelling equilibrates. This function is usually referred to as "swelling kinetics" which coincides with desorption kinetics.

This process comprises a few stages including diffusion. But diffusion is so long as compared to the other process that analyzing kinetics of the desorption we can only concentrate on the kinetics of diffusion. It is for this reason that mathematical models describing diffusion are often used to interpret sorption kinetics. Among these interpretations one can distinguish a Ruckenstein bidisper diffusion model [33], the Fickian diffusion and relaxation model [34], quasi-permanent diffusion model [35], double exponential model [36] and an extended exponential model combining the characteristic speed parameter with the stretch parameter [37].

If we consider transport of gas in the whole coal seam, despite significant analogies to diffusion, many researchers describe transport mechanisms as filtration in Darcy's approach, or in the case of a more complex description as filtration with slippage effect in Klinkenberg's approach.

In order to quantify the kinetics of the combined sorption and diffusion processes of sorbate in coal, the solution proposed by Crank, often called the unipore model is most often used [38,39]. It is based on Fick's laws supplemented with a sorption factor represented by a linear sorption isotherm. In his work, Crank indicates analytical solutions in the form of expanding in series for spherical grains, cylinders and plane sheet.

Transport kinetics studied in laboratory conditions is mainly observed in granular samples. This is due to the ease of preparation of the appropriate sample by selecting the tested grain size. The grains within the grain class are treated as spheres, represented by the so-called equivalent radius [40].

Desorption of sorbate from coal is time-consuming. Figure 1a,b present a demonstration time period in which half of the total CO₂ content is emitted from the coal samples with $D_e = 10^{-9}$ cm²/s with equivalent radii in the range of 0.007–0.15 cm (Figure 1a) and 0.007–1.5 cm (Figure 1b). Even in the case of small grains, if the most typical values of effective diffusion coefficients are taken into account, this process can last from several hours for grains below 0.01 cm, through several weeks for millimeter grains, to months and years for centimeter and larger samples. The kinetics of CO₂ desorptions depend on the second power of the grain equivalent radius.

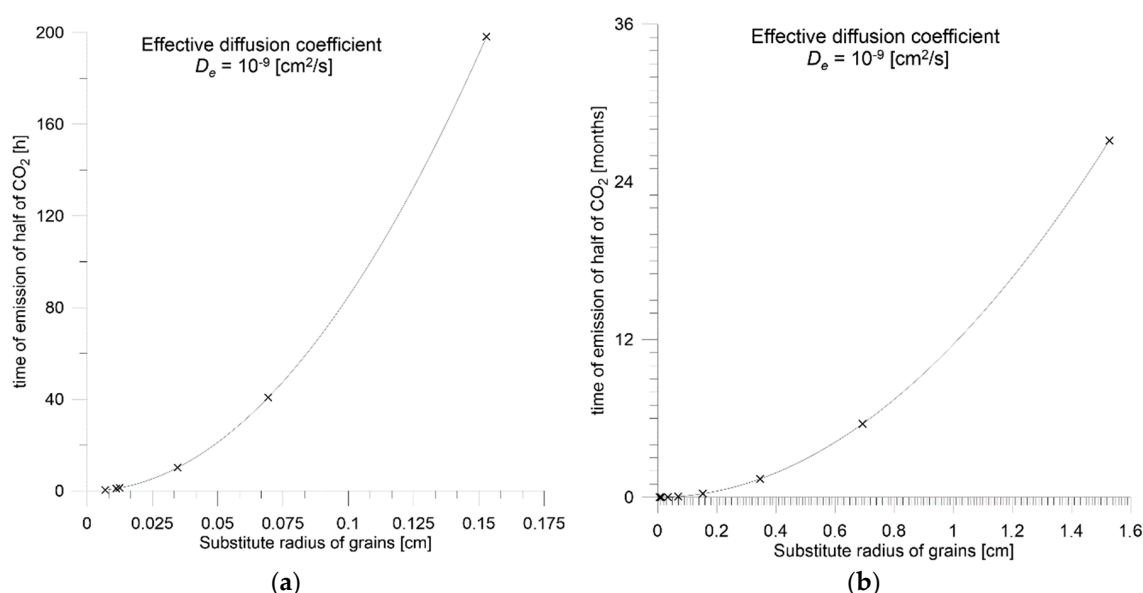


Figure 1. The half time of CO₂ desorption from coal samples $D_e = 10^{-9}$ [cm²/s] of various equivalent radii in the range of: (a) 0.007–0.15 cm; (b) 0.007–1.5 cm.

Obtaining complex shapes of coal samples is difficult, and the desorption of gas sorbate for large samples is long-lasting. It is for this reason that the number of studies on the kinetics of gas sorbate

desorptions from non-granular coal samples is small. The authors used carbon samples with a cuboid shape and a thickness much smaller than the other two dimensions of this solid. This approach allows the solution of Crank's equations for plane sheet. It will also compare the results of diffusion coefficient tests for this type of samples with tests on spherical samples. In addition, due to the relatively small sample thickness, it is possible to record the full course of the process in an acceptably short time. With plane sheet samples, it is also possible to contact sample contraction during desorption without contact.

2. Research Methodology

Coal from two coal mines in Poland was selected for testing. The coal material was divided into two groups. Part of the coal was crushed and sieved to separate the grain size of 0.2–0.25 mm (Figure 2a). From the other part samples were prepared on a laboratory polisher whose height and width were much greater than the depth. The minimum achievable thickness of the samples was about 0.6 mm (Figure 2b), with a height and width of about 20 mm. Due to the significant disproportion of height and width dimensions to the depth, the prepared sample was considered a plane sheet.

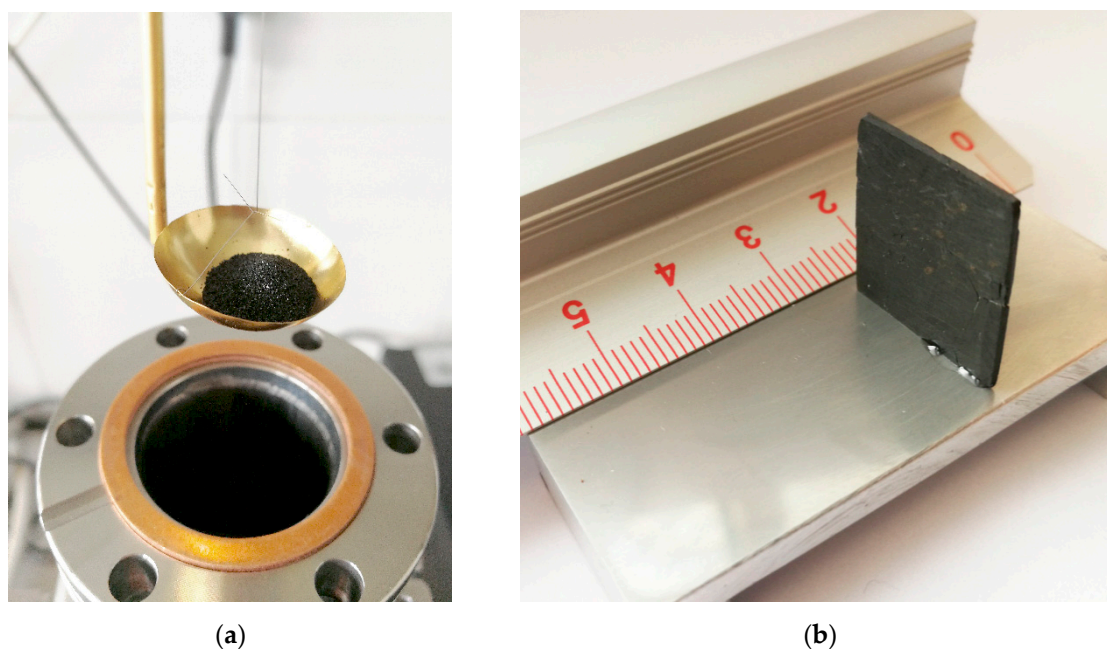


Figure 2. Coal sample: (a) after grinding to 0.2–0.25 mm grains; (b) plane sheet.

Crushed and sieved samples with the grain size of 0.2–0.25 mm were subjected to technical and petrographic tests as well as structural and sorption tests. Technical analyses of volatile matter, ash and moisture content were made based on Polish-ISO standards PN-ISO 562: 2000, PN-ISO 1171 that comply with the European standards. The content of macerals in coal was determined by petrographic methods through quantitative analysis using reflected light microscopy.

Structural tests of the samples were performed on an ASAP 2020 volumetric analyzer (Micromeritics, Norcross, Georgia, USA). The samples were subjected to low-pressure gas adsorption (LPA) tests in isothermal conditions, in the absolute pressure range of 0–0.1 MPa. Carbon dioxide at 273 K and nitrogen at 77 K were used as the adsorbates. CO₂ adsorption was measured in the relative pressure range: $0 < p/p_0 < 0.029$. The relative pressure was determined as the ratio of the absolute pressure and the saturation pressure of the gas used. At the preparation stage, the samples were degassed for 12 h at 363 K and then heated for 4 h (368 K). During N₂ adsorption, the relative pressure range was $0 < p/p_0 < 0.996$ respectively. Prior to measurement, samples were degassed for 2 h (363 K). The LPA measurement involved measuring the volume of the sorbed gas in the sample pore space. On the basis of equilibrium adsorption points, the area of micropores and partly mesopores was

characterized in the tested coals. The study determined the total sorption capacity, monolayer and multilayer specific surface area (SSA), pore volume and average pore size and distribution. In the LPA process, Langmuir, Horvath–Kawazoe (HK) [41], density functional theory (DFT) [42] and Dubinina Astakhova (DA) [43] models were used for calculations using CO₂ adsorbate, while with the use of N₂ adsorbate, Brunauer-Emmett-Teller (BET) [44] and Barrett-Joyner-Halenda (BJH) [45] respectively.

Skeletal density was determined on an AccuPyc II 1340 helium pycnometer (Micromeritics, Norcross, Georgia, USA). This parameter was necessary for sorption tests which were made on a sorption analyzer IGA001 (Hidden Isochema, Warrington, UK). Sorption isotherms were determined at 293K.

In the case of grain samples, the measurement included the recording of changes in the mass of coal samples under the influence of methane sorption for the following pressures: 0.1 MPa, 0.5 MPa and 1.5 MPa. At the preparation stage, the sample was degassed for 24 hours in a high vacuum obtained by a turbomolecular pump (10⁻⁷ Pa) at 353K. On the basis of sorption points, Langmuir sorption isotherms were determined by minimizing the sum of squared deviations (1):

$$a(P) = \frac{A \cdot B \cdot P}{1 + B \cdot P}, \quad (1)$$

where $a(P)$ is sorption equilibrium point, (cm³/g), A is total monolayer capacity, (cm³/g), B is the inverse of the half pressure, (1/MPa), P is absolute pressure (MPa).

In the case of plane sheet samples, a change in the sample mass was recorded, following a quasi-step pressure reduction from 1.0 MPa to 0.1 MPa at 293 K. The preparation stage included degassing the sample for 10 days in a high vacuum obtained by a turbomolecular pump (10⁻⁷ Pa) at 353 K.

MicroEpsilon measuring laser sensor with a height measuring range of ±5000 µm and a resolution of 1 µm was used in the study of sample size changes (Figure 3)

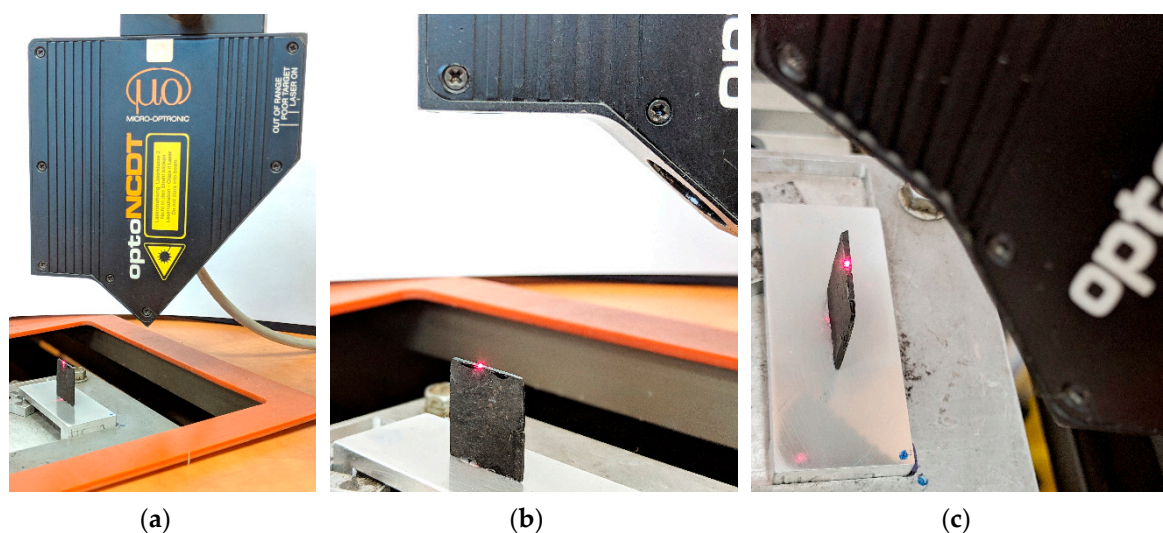


Figure 3. Registration of changes in the plane sheet sample geometry during desorption: (a) measuring laser head; (b) side view of the sample; top view of the sample.

The sensor was mounted on a rigid plinth equipped with a micrometer screw that allows vertical movement and stops the device at the desired height relative to the measured sample. The device was placed on a marble slab in order to eliminate the influence of possible ground vibrations on the measurement results. The distance was measured on a triangulation basis. The laser beam emitted by the sensor was reflected from the tested surface. A particle of such reflected light returned to the sensor, where through the lens system it was focused on the photosensitive measuring element. As a

result of the measurement, the device returned the numerical value of the distance of the tested surface from the laser sensor. The device was turned on an hour before the start of the main measurements to eliminate the influence of its heating on possible measurement errors. The measurement took place in a thermostatic room at 293 K.

Before the measurement of geometry changes during desorption, the plane sheet coal samples were sealed in an airtight pressure container. Vacuum was maintained in the container for 10 days. Then the hermetic container was filled with CO₂ to a pressure of 1 MPa. The sample was saturated with CO₂ at a given pressure for another 10 days. Then, the pressure in the container was abruptly lowered to atmospheric pressure. The pressure change began desorption and contraction of the sample. Within a few dozen of seconds of the pressure drop, the sample was placed under the laser sensor, which began the measurement of the changes in the sample's geometry.

To include sample size changes $\Delta z(t)$ in the first seconds of CO₂ desorption, in the time between the pressure drop in the airtight container and the moment the sample is placed under the laser altimeter (Figure 4a,b), an approximation of the square root curve was performed (2):

$$\Delta z(t) = a \cdot \sqrt{t} + c, \quad (2)$$

where $\Delta z(t)$ is sample size changes, a is sorption capacity, t is time.

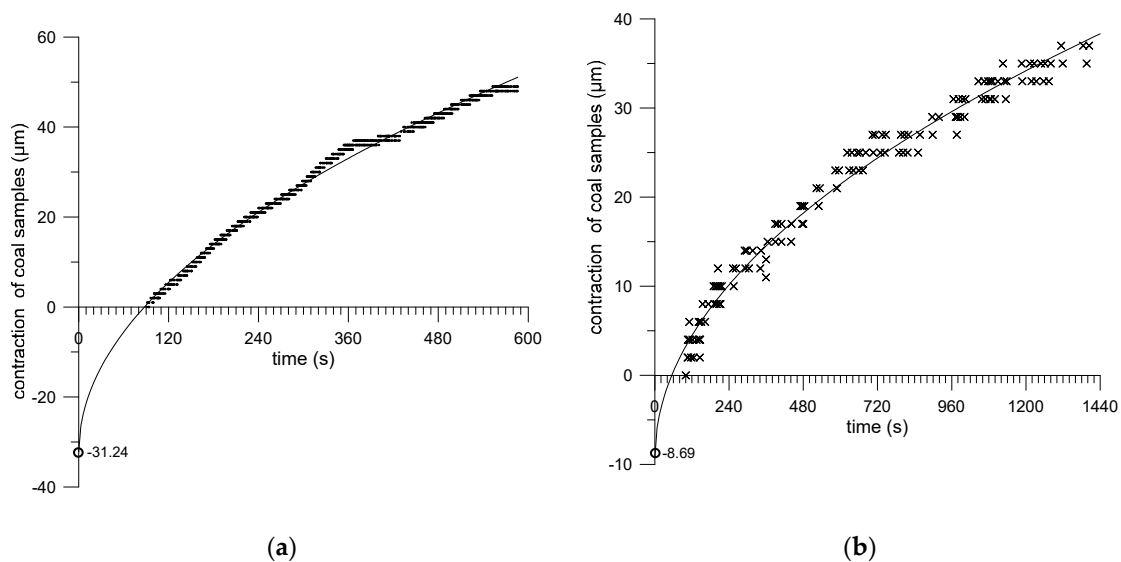


Figure 4. Taking into account changes in the size of coal samples during desorption in the time between the step change in pressure, with the moment of recording the sample geometry: (a) coal from Sobieski mine coal; (b) coal from Budryk mine coal.

The root curve well describes the kinetics of sorbate desorptions from coal at the beginning of the process, as indicated by [46].

3. Petrographical and Structural Description of Analyzed Coal

Coals from Sobieski mine and Budryk mine in Poland were used in the research. Coal samples were taken as part of the years of cooperation between the Strata Mechanics Research Institute of the Polish Academy of Sciences and Polish hard coal mines. They differed in petrographic structure and technical composition. On the basis of vitrinite average reflectivity R_o , according to the International Classification of In-Seam Coals classification [47] both coals were air-dried medium-rank C Ortho-bituminous coal. In terms of ash content, the coal from Sobieski mine was classified as medium grade coal, and the coal from Budryk mine was classified as high grade coal. Coal parameters

are summarized in Table 1. The coal from Sobieski mine has a lower vitrinite reflectivity value and an almost 10% higher vitrinite content.

Table 1. Technical and petrographic parameters of the tested coals.

Coal	R_0 (%)	Vitrinite (%)	Inertinite (%)	Liptinite (%)	V^{daf} (%)	A^d (%)	W^t (%)	ρ_{sk} (g/cm ³)
Sobieski mine	0.71	73.7	16.8	9.5	32.35	11.54	5.35	1.44
Budryk mine	0.85	62.6	27.0	10.4	30.98	8.40	1.22	1.37

where R_0 is vitrinite reflectivity, V^{daf} is volatiles, A^d is ash, W^t is moisture, ρ_{sk} is skeletal density.

Using the LPA method and CO₂ as the adsorbate, the ultra-micropores and micropores in coal were characterized. N₂ was used as the adsorbate to characterize the mesopores. On the basis of equilibrium points of CO₂ adsorption, sorption type I isotherm was obtained according to the IUPAC [3]. This shape is similar to the Langmuir isotherm model and is characteristic of microporous materials. N₂ adsorption points were consistent with type III isotherm according to IUPAC classification [3]. This shape is typical for low porosity materials. The differences in the shape of CO₂ and N₂ isotherms result from the different sorption potential of these gases. Nitrogen exhibits weak sorption activity to coal. The kinetic diameter of CO₂ is smaller and coal has a higher sorption affinity to the molecules of this gas. Consequently, CO₂ is able to permeate into ultra-micropores with diameters as small as 0.4 nm that are inaccessible to nitrogen [48]. CO₂ and N₂ adsorption isotherms of coal are presented in Figure 5 and the calculation results are shown in Table 2.

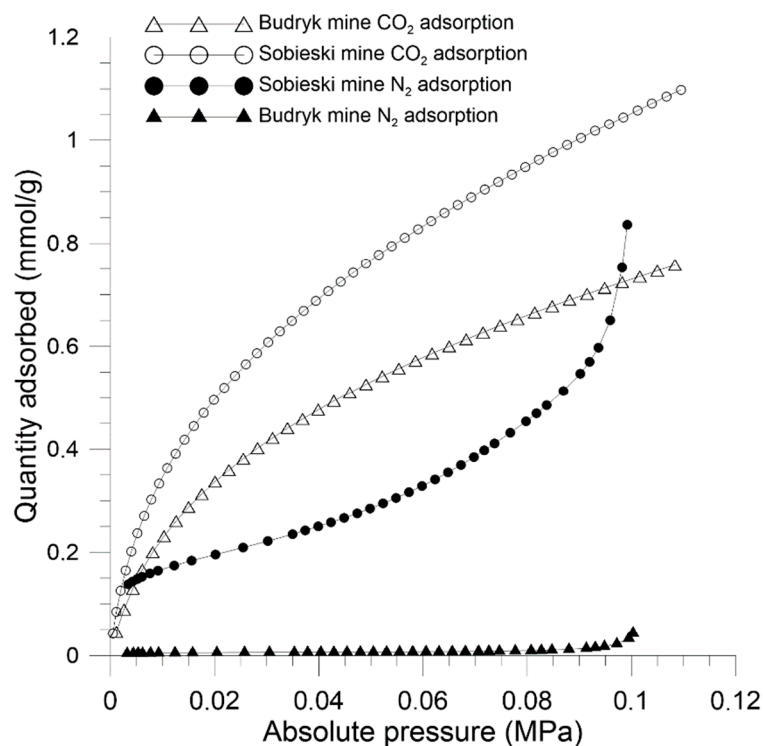


Figure 5. CO₂ adsorption isotherms (273 K) of coal materials.

Table 2. Structural parameters of coal materials during CO₂ adsorption.

CO ₂ Adsorption, 273K	Sobieski Mine	Budryk Mine
Langmuir total sorption capacity (mmol/g)	1.554	1.117
Langmuir specific surface area (m ² /g)	159.09	114.38
HK maximum pore volume (cm ³ /g)	0.045	0.031
HK average pore width (nm)	0.665	0.668
DFT volume in pores < 0.43 nm, * 10 ⁻³ (cm ³ /g)	0.96	1.80
DFT total pore volume ≤ 1.08 nm, * 10 ⁻³ (cm ³ /g)	32.77	24.71
DFT pore area > 1.08 nm, (m ² /g)	92.28	61.51
DFT total pore area ≥ 0.43 nm, (m ² /g)	197.70	130.21
DA characterization of adsorption energy, (kJ/mol)	20.70	20.11
DA volume of micropores (cm ³ /g)	0.09	0.06
DA surface area of micropores (m ² /g)	224.10	149.28
N ₂ Adsorption, 77K		
Sorption capacity (mmol/g)	0.836	0.044
BET specific surface area (m ² /g)	15.42	0.43
BJH total pore volume (cm ³ /g)	0.027	0.001
BJH specific surface area (m ² /g)	10.79	0.20
BJH average pore diameter (nm)	9.85	27.56

where: HK is Horvath–Kawazoe model; DFT is density functional theory; DA is Dubinin–Astakhov model; BET is Brunauer–Emmett–Teller model; BJH is Barrett–Joyner–Halenda model.

Structural analysis showed that the tested coals differ in their structure. Sobieski mine coal obtained a total Langmuir sorption capacity equal to 1.554 mmolCO₂/g, which is higher than in the case of Budryk mine coal (1.117 mmolCO₂/g). The Sobieski mine coal also obtained a higher SSA Langmuir value and a much higher SSA value in terms of micropores (DA model). This value was high compared to typical SSA levels coals [9,17]. The total volume of micro and ultra-micropores in coals, according to the HK theory, was in the range of 0.031 cm³/g to 0.045 cm³/g, while according to the DA theory, in the range of 0.06–0.09 cm³/g, respectively. The average width of the pores accessible to CO₂ was 0.67 nm, which corresponds to the range of ultra-micropores in the materials (0–0.8 nm). The characteristic adsorption energy, determined according to DA theory, interpreted as the energy barrier needed to overcome the dispersion forces between adsorbate and coal molecules, was slightly higher in Sobieski mine coal and amounted to 20.70 kJ/mol, while in Budryk mine coal it was 20.11 kJ/mol.

The differences in the values of structural parameters affect the sorption capacity and result, among others from different proportions of macerals in coals. Coals with a high content of vitrinite macerals, such as the ones from the Sobieski mine, have a more extensive structure in the range of micropores and ultramicropores and achieve higher values of structural and sorption parameters. In coals with a high content of intertinite macerals, as in Budryk mine, a large proportion of micropores and mesopores is noted. This affects lower values of pore volume and specific surface area. This is confirmed by studies based on CO₂ adsorption. The pore size distribution of the tested coals was determined according to the HK model. It is presented in Figure 6. In Sobieski mine coal with a higher vitrinite content, a larger pore volume was obtained in the entire studied range of micropore diameters. The cumulative pore volume in Sobieski mine was 50% higher than Budryk mine (Figure 6).

On the basis on the LPA results using N₂, pore distribution was determined using the BJH model. Also in the range of mesopores (2–50 nm) Sobieski mine had a larger pore volume than Budryk mine in the entire diameter range. The largest volume was found in pores with diameters above 30 nm. It is presented in Figure 7.

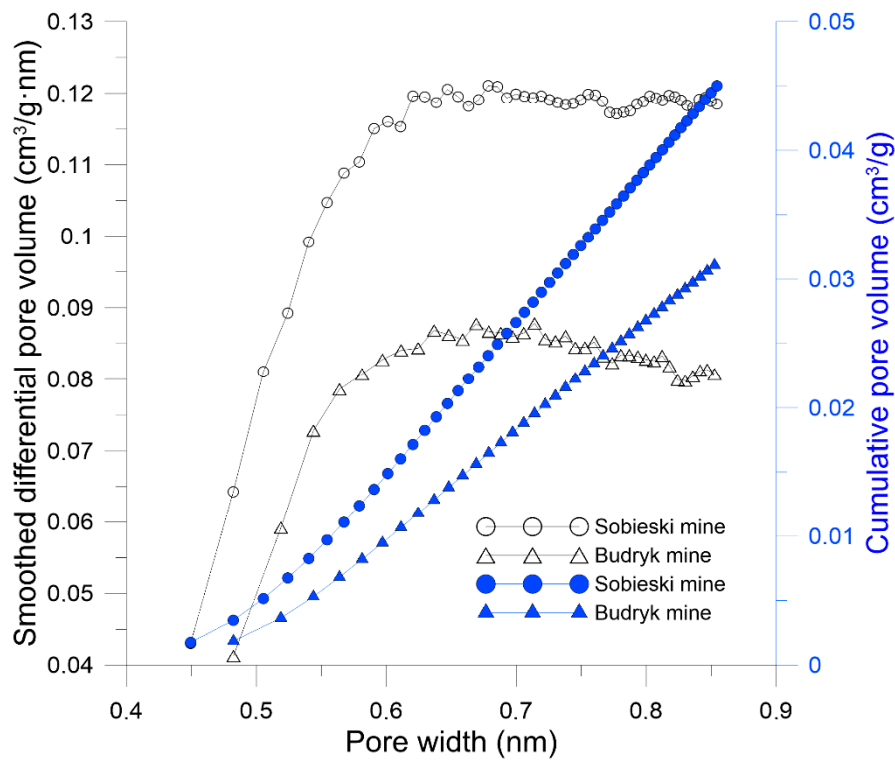


Figure 6. Pore size distribution of the coals based on method low-pressure gas adsorption (LPA) CO₂ (HK model).

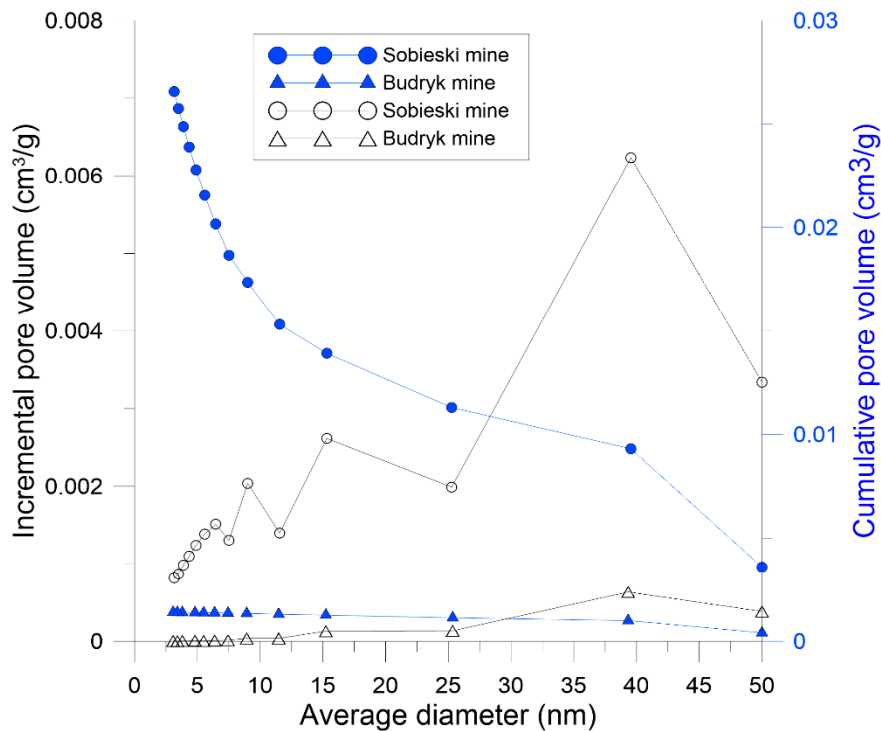


Figure 7. Pore size distribution of coals based on method LPA N₂ (BJH model).

4. Gas Desorption from the Spherical Coal Sample

The sorbate accumulation/desorption mechanism within individual sorbent grains consists of several stages. These include the transport of the sorbate component to the particle surface, diffusion in

the pores and the actual sorption process. In the description of the kinetic model of the sorption process, the diffusion stage is assumed as the dominant factor. In the considerations regarding the combined sorption and transport processes of gas sorbate that occur during the saturation of porous sorbent grains, it is assumed that within the sorbent pore system mobile gas sorbate and bound sorbate coexist. Transport takes place with the use of mobile sorbate, and the amount of bound sorbate determines the level of adsorption. It is assumed that the accumulation process takes place while maintaining the local sorption equilibrium, which can be described by Henry's linear isotherm. The accumulation process starts at the moment t_0 as a result of a step change in external conditions, after which these conditions remain unchanged. The accumulation process is accompanied time changes of the distribution of the cumulative concentration C of the sorbate within grains. If it is assumed that a linear sorption isotherm can be used, the accumulation process can be described using Fick's second law:

$$\frac{\partial c}{\partial t} = D_e \nabla^2 C, \quad (3)$$

but

$$D_e = \frac{D}{1 + H'}, \quad (4)$$

where D_e is effective diffusion coefficient, C is cumulative concentration of the sorbate, D is diffusion coefficient.

In Equation (3), the diffusion coefficient D is replaced by an effective diffusion coefficient D_e . The value of this coefficient results from the diffusion coefficient value D and the inclination of Henry's isotherm.

4.1. Mathematical Model of Desorption

In the case of a sphere with a radius R (Figure 8) Equation (3) takes the form:

$$\frac{\partial u}{\partial t} = D_e \frac{\partial^2 u}{\partial r^2}, \quad (5)$$

while $u = r \cdot C(r, t)$, r is the distance from the center of the sphere, $C(r, t)$ is distribution of sorbate concentration within it.

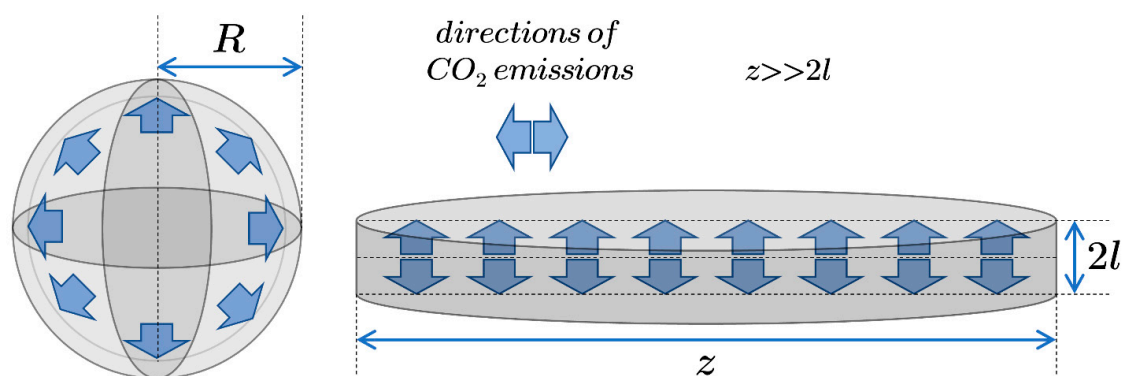


Figure 8. Methane desorption from spherical grains and plane sheet samples.

The solution of Equation (5) takes the form:

$$\frac{C(r, t) - C_1}{C_0 - C_1} = 1 - \frac{2R}{\pi r} \sum_{n=1}^{\infty} \frac{(-1)^n}{n} \exp\left(-t \frac{D_e (\pi n)^2}{R^2}\right) \sin\left(r \frac{\pi n}{R}\right), \quad (6)$$

where constants C_1 and C_0 determine the average concentration of sorbate in grain before and after the process is completed.

Mass $M(t)$ the substance accumulated in the spherical grain tends to the limit value M_∞ according to the formula:

$$\frac{M(t)}{M_\infty} = 1 - \frac{6}{\pi^2} \sum_1^{\infty} \exp\left(-\frac{n^2\pi^2 D_e t}{R^2}\right). \quad (7)$$

Equation (7) is often used to determine the value of the effective diffusion coefficient based on the recording of the sorbate accumulation process by spherical sorbate grains. In the case of coal, the diffusion coefficient determined on its basis is an important parameter for assessing the state of methane hazards and gas and rock outbursts in mines. Knowledge of this parameter is also necessary when considering the degassing of seams and aspects related to sequestration and underground storage of carbon dioxide.

4.2. Laboratory Measurements

In accordance with the described measurement methodology, sorption isotherms for granular samples were plotted: Sobieski mine (Figure 9) and Budryk mine (Figure 10). Sorption capacities at individual pressures and Langmuir sorption isotherm parameters are presented in Table 3.

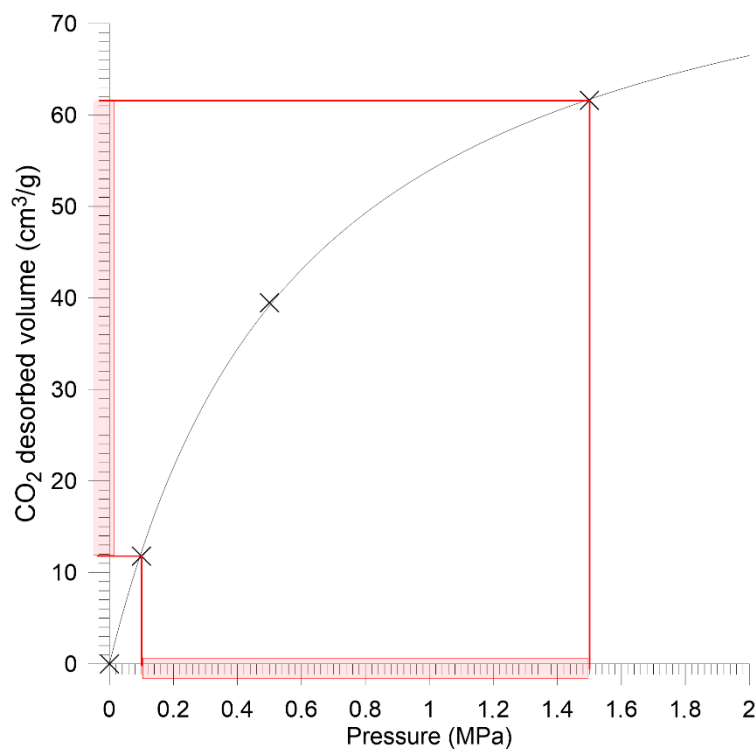


Figure 9. Sorption isotherm for Sobieski mine coal—granular sample.

Table 3. Sorption parameters of tested granular samples.

Coal	Sorption Capacities			Parameters of the Langmuir Isotherm		Effective Diffusion Coefficient
	$a(0.1)$	$a(0.5)$	$a(1.5)$	A	B	D_e
	(cm^3/g)	(cm^3/g)	(cm^3/g)	(cm^3/g)	($1/\text{MPa}$)	(cm^2/s)
Sobieski mine	11.78	39.48	61.48	86.70	1.65	3.51×10^{-8}
Budryk mine	6.24	14.18	20.89	25.46	2.76	6.58×10^{-9}

where $a(0.1)$, $a(0.5)$, $a(1.5)$ is sorption capacity at 0.1 MPa, 0.5 MPa and 1.5 MPa pressure; A is total sorption capacity of the monolayer, B is inverse of half pressure; D_e is effective diffusion coefficient.

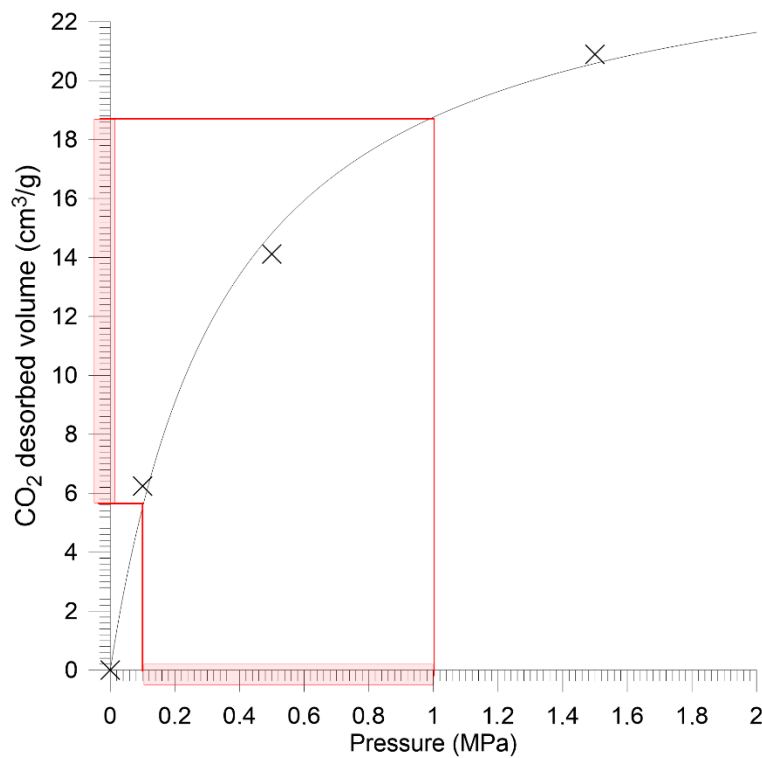


Figure 10. Sorption isotherm for Budryk mine coal—granular sample.

In terms of sorption properties, the analyzed coals differed significantly. According to Langmuir (1), the monolayer sorption capacity of coal from Sobieski mine had was over 3 times higher than in the case of Budryk mine coal.

The kinetics of CO₂ saturation in spherical coal samples was analyzed. Interpretations included changes in the mass of coal samples after a quasi-step change in pressure from a vacuum to 0.1 MPa. Direct results of measurements of Sobieski mine coal are presented in Figure 11 and of Budryk mine coal in Figure 12.

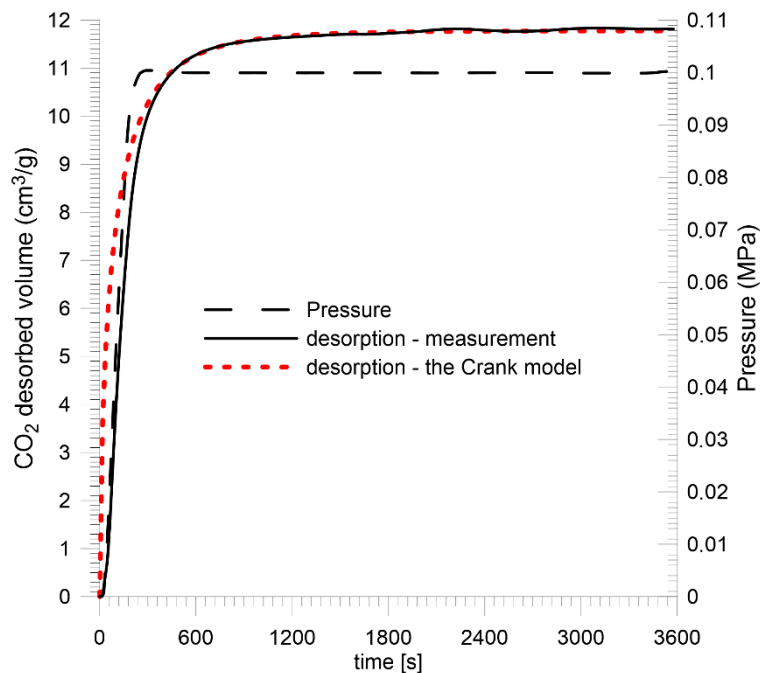


Figure 11. CO₂ saturation kinetics for Sobieski mine coal—granular sample.

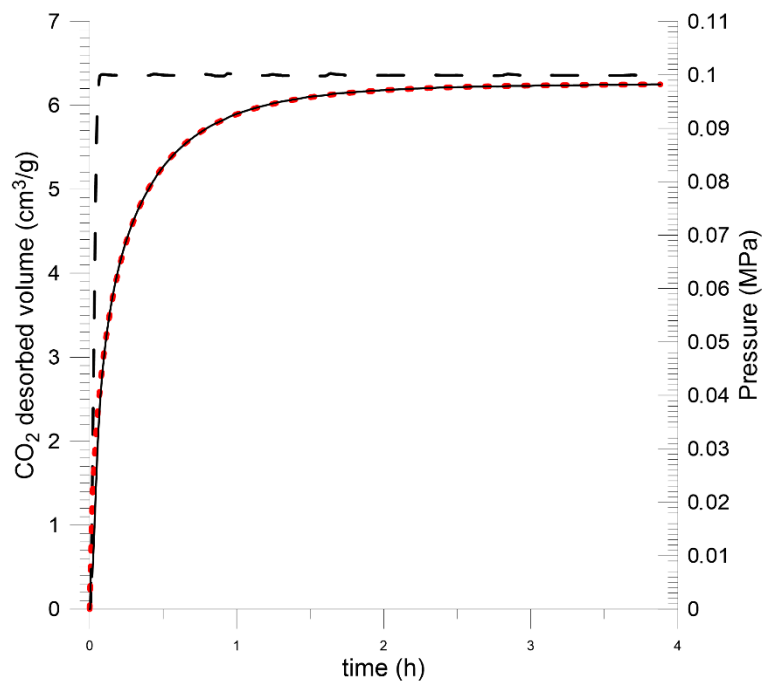


Figure 12. CO₂ saturation kinetics for Budryk mine coal—granular sample.

Measurement data was approximated by the method of the least squares according to the Crank model for the sphere (7). The equivalent radius for the 0.2–0.25 mm grain size was 0.011 mm. The quantitative approach to saturation kinetics also indicates huge differences between the studied coals. The effective diffusion coefficient takes the value less than ten times higher in the case of Sobieski mine coal compared to Budryk mine coal (Table 3).

5. Gas Desorption from the Plane Sheet Coal Sample

The opposite of a spherical sample is a plane sheet. We deal with this type of a geometric model when one dimension is significantly smaller than the others. In the case of a diffusion model of a sorbate from a porous sorbent for the plane sheet layer, Crank provides a solution in the form of a series expansion.

5.1. Mathematical Model of Desorption

For a layer size of $2l$, y , z , where the sizes $y \gg 2l$ and $z \gg 2l$, Equation (3) takes the form:

$$\frac{\partial u}{\partial t} = D_e \frac{\partial^2 u}{\partial x^2}, \quad (8)$$

but

$$u = x \cdot C(x, t), \quad (9)$$

where x is the distance from the center of dimension x , $-1 < x < 1$, $C(x, t)$ is distribution of sorbate concentration within it.

Where the value of the coefficient D_e remains unchanged, as a result of the process caused by a step change in the conditions in the sorbent environment, the concentration of the accumulated substance C changes from C_0 to C_1 and mass $M(t)$ of the sorbate introduced into the selected fragment of sorbent is from M_0 to the limit value M_∞ . For a flat-parallel layer with thickness $2l$, the solution

of the diffusion Equation (10) determines the changes in the distribution of sorbate concentration in the layer:

$$\frac{C(x^*, t) - C_0}{C_1 - C_0} = 1 - 4 \sum_{n=0}^{\infty} \left(\frac{(-1)^n}{A_n} \exp\left(-t \frac{D_e A_n^2}{4l^2}\right) \sin\left(\frac{x}{2l} A_n\right) \right), \quad (10)$$

where x^* and x are the distance from the plane of symmetry and the edge of the layer, but: $A_n = \pi(2n + 1)$.

Mass $M(t)$ of the sorbate introduced into the selected fragment of the flat parallel layer is:

$$\frac{M(t)}{M_{\infty}} = 1 - \sum_{n=0}^{\infty} \frac{8}{A_n^2} \exp\left(-t \frac{A_n^2 D_e}{l^2}\right). \quad (11)$$

5.2. Laboratory Measurements

For plane sheet samples, the sample saturation kinetics were recorded at a quasi-step change in CO_2 pressure from vacuum to 1.0 MPa. Prior to that, the samples were prepared in a vacuum for 10 days. Direct results are presented in Figures 13 and 14 and in Table 4.

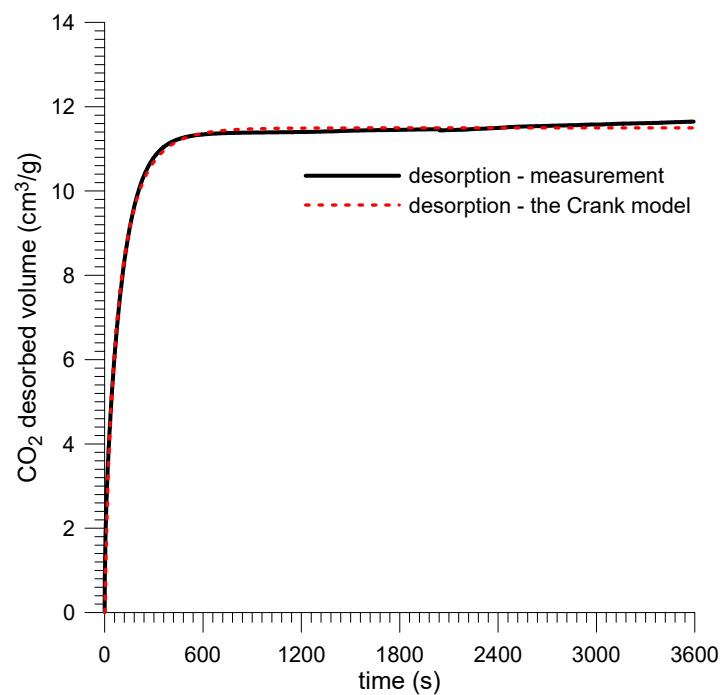


Figure 13. CO_2 saturation kinetics for Sobieski mine coal—plane sheet sample.

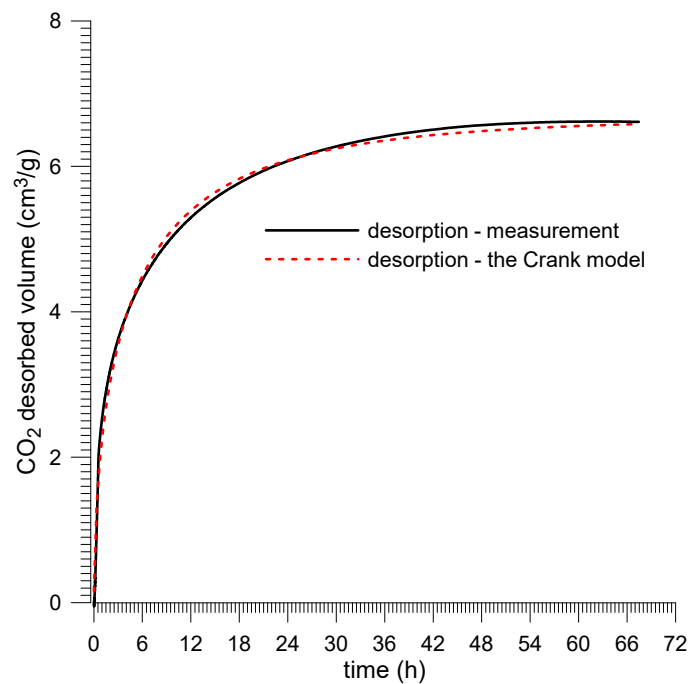


Figure 14. CO₂ saturation kinetics for Budryk mine coal—plane sheet sample.

Table 4. Sorption parameters describing CO₂ desorption from granular samples and the plane sheet type described by an appropriate mathematical model.

Coal	Sorption Capacity			Effective Diffusion Coefficient						
	Spherical Samples	Plane Sheet Samples	Percentage Difference	Spherical Samples	Plane Sheet Samples	Percentage Difference	Spherical Samples	Plane Sheet Samples		
	$a(0.1 \text{ MPa}), (\text{cm}^3/\text{g})$		(%)	$D_e, (\text{cm}^2/\text{s})$		(%)	$RSoS$	R^2	$RSoS$	R^2
Sobieski mine	11.55	11.78	1.95	3.51×10^{-8}	3.92×10^{-8}	-11.68	183	0.982	125	0.989
Budryk mine	6.24	6.24	0	6.58×10^{-9}	7.25×10^{-9}	-10.18	167	0.088	97	0.995

where: $RSoS$ —residual sum of squares, R^2 —coefficient of determination, R -squared.

The measurement data were approximated by the Crank model using the least squares method for the plane sheet sample (11). It was assumed that the average thickness of the sample layer was $2l = 0.6$ mm.

6. Accompanying Coal Shrinkage

Shrinkage of unloaded coal samples was observed using a laser altimeter. The sample was saturated with CO₂ in an external tank and immediately placed under the head of the altimeter. The CO₂ desorption process and the accompanying shrinkage were triggered by a step change in the gas pressure from saturation pressure to atmospheric pressure. The recorded changes in the sample size are shown in Figures 15 and 16.

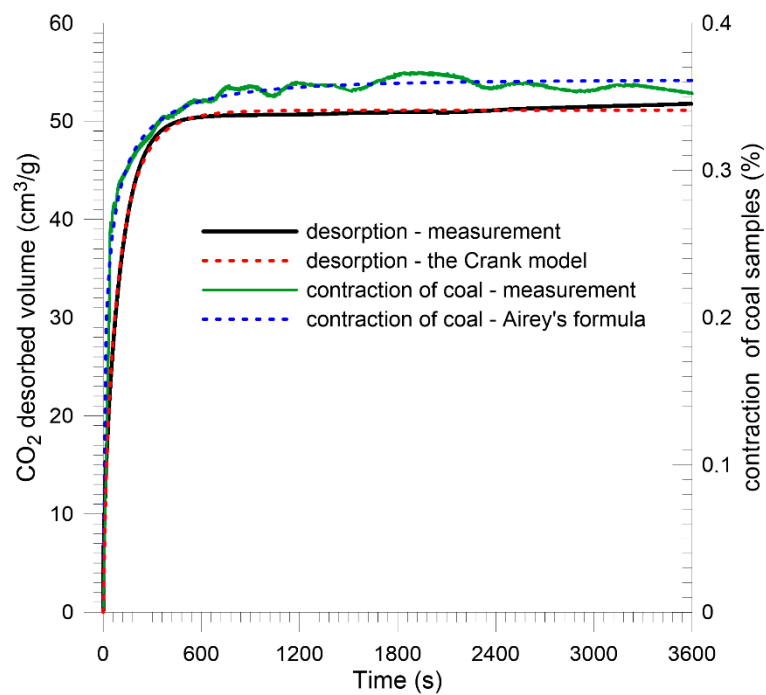


Figure 15. Kinetics of shrinkage of Sobieski mine coal juxtaposed with CO₂ desorption kinetics—plane sheet sample.

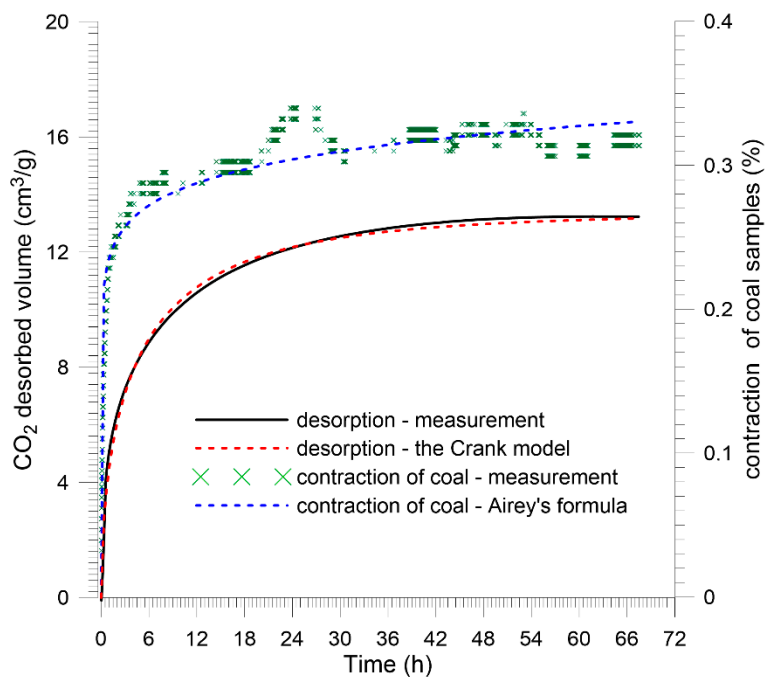


Figure 16. Kinetics of shrinkage of Budryk mine coal juxtaposed with CO₂ desorption kinetics—plane sheet sample.

Measurement data were extrapolated by the Airey formula [49]:

$$\frac{X(0) - X(t)}{X(0) - X(\infty)} = A - Be^{-\left(\frac{t}{\tau}\right)^C}, \tag{12}$$

where: $X(0)$, $X(t)$ and $X(\infty)$ is the sample size in the following order: sorption equilibrium, at the moment t of gas desorption from the sample and the asymptotic value. C and T are phenomenological coefficients.

Graph analysis indicates that the asymptotic value of the sample shrinkage in both cases was about 0.35%. The kinetics of size changes differed significantly for the coals tested, as did the CO_2 desorption kinetics. It is also worth noting that for individual coals, shrinkage kinetics is clearly faster than the kinetics of CO_2 desorption. Measurement by a gravimetric device assumes that the change in mass is recorded when the gas molecule is bound to the porous material by surface interaction forces. The fact that the recorded shrinkage of the material occurs faster than the change in sorbent mass under the influence of sorption may suggest that the start of surface diffusion (Volmer) and solid diffusion have a slow effect on the cumulative change in sample mass, but significantly change the size of the sample. Figure 17 shows particular types of diffusion in the coal pore system. During surface diffusion and solid diffusion, gas molecules move, but remain in quasi-continuous contact with the sorbent surface.

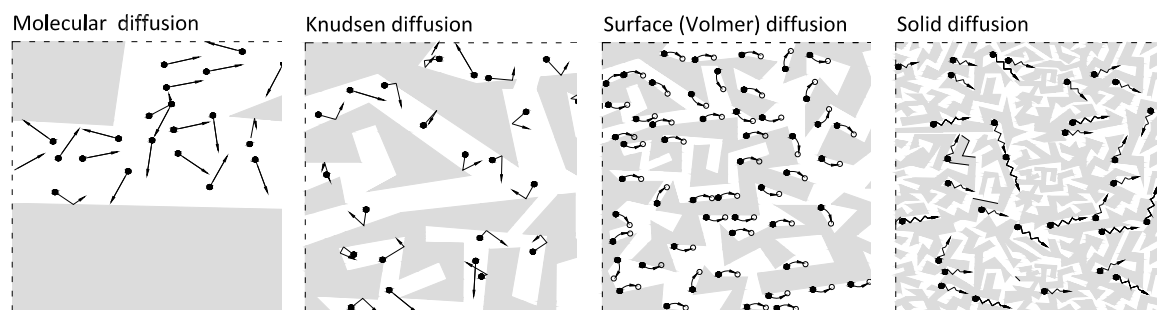


Figure 17. Particular types of diffusion in the coal pore system [50].

7. Conclusions

The paper presents studies on two coal samples from Polish mines, differing in petrographic and structural parameters. It was shown that the tested coals differed in structural structure. Structural parameters of micropores had much higher values in Sobieski mine coal, which had 10% higher vitrinite content than Budryk mine coal, and lower vitrinite reflectivity. The Sobieski mine sample obtained a higher SSA value, both in terms of the Langmuir monolayer model and the BET and BJH multilayer model. The cumulated volume of ultramicropores (HK model) was nearly 50% larger in the Sobieski mine coal than in Budryk mine coal, while the cumulated volume of mesopores here was several dozen times higher.

The authors examined CO_2 desorption on grain coal samples of a sphere-like shape and a plane sheet shape. The desorption time of gas sorbate from coal depends on the square of the sample size. Sorption tests are usually carried out on small granular samples up to about 1 mm, because such samples ensure the achievement of sorption equilibrium within a few days. However, with such small samples it is difficult to test shrinkage/swelling that result from sorption. The use of plane sheet samples allowed shortening the measurement time to several days, due to the fact that the gas desorption occurred in the geometrically shortest direction (about 1 mm). At the same time, it was possible to observe the coal shrinkage, since the longest sample size of coal was over 20 mm.

The Crank model obtained for spherical grains and plane sheet samples was extrapolated from the registered CO_2 desorption kinetics. Literature review reveals that so far no sorption analysis results have been extrapolated with a Crank model other than for spherical grains.

The values of the R -squared coefficient and the values of the sum of squared deviations of the model fitting to the measured values (Table 4) indicate that the plane sheet model does not describe the course of CO_2 desorption from such samples worse than the commonly used unipor model for

granular samples. This result may be related to the fact that the roundness of the sieved coal grains is only statistical, while the shape of the plane sheet samples is more consistent with the model shape.

In the tested plane sheet samples, the material shrinkage during desorption was observed to be approximately 0.35% in both cases. In the case of both tested coals, it can be observed that the dilatometric reaction is faster than the combined desorption and diffusion processes recorded by the sorption analyser.

Author Contributions: Conceptualization, M.M.; methodology, N.S., M.M. and A.P.; software, N.S.; validation, N.S.; formal analysis, N.S. and A.P.; investigation, N.S.; resources, N.S.; data curation, N.S. and A.P.; writing—original draft preparation, N.S. and A.P.; writing—review and editing, M.M. and A.P.; visualization, N.S. and A.P.; supervision, M.M.

Funding: This research received no external funding.

Acknowledgments: The present work was financed by the AGH—University of Science and Technology, Faculty of Geology, Geophysics and Environmental Protection and The Strata Mechanics Research Institute of the Polish Academy of Sciences as a part of statutory projects.

Conflicts of Interest: The authors declare no conflict of interest.

References

1. Godyn, K.; Kozusnikova, A. Microhardness of Coal from Near-Fault Zones in Coal Seams Threatened with Gas-Geodynamic Phenomena, Upper Silesian Coal Basin, Poland. *Energies* **2019**, *12*, 1756. [[CrossRef](#)]
2. Godyn, K. Structurally altered hard coal in the areas of tectonic disturbances—an initial attempt at classification. *Arch. Min. Sci.* **2016**, *61*, 677–694.
3. IUPAC Physical Chemistry Division Commission on Colloid and Surface Chemistry Subcommittee on Characterization of Porous Solids. Recommendations for The Characterization of Porous Solids (Technical Report). *Pure Appl. Chem.* **1994**, *66*, 1739–1758. [[CrossRef](#)]
4. Sing, K.S.W.; Everett, D.H.; Haul, R.A.W.; Moscou, L.; Pierotti, R.A.; Rouquerol, J.; Siemieniowska, T. Reporting Physisorption Data for Gas/Solid Systems with Special Reference to the Determination of Surface Area and Porosity. *Pure Appl. Chem.* **1985**, *57*, 603–619. [[CrossRef](#)]
5. Mahajan, O.P.; Walker, P.L. *Porosity of Coal and Coals Products*; The Pennsylvania State University: Philadelphia, PA, USA, 1978.
6. Ettinger, J.L. Solubility of Methane Contained in Coal Deposits. *Arch. Min. Sci.* **1990**, *33*, 35.
7. Skiba, M.; Młynarczuk, M. Identification of Macerals of the Inertinite Group Using Neural Classifiers, Based on Selected Textural Features. *Arch. Min. Sci.* **2018**, *63*, 827–837.
8. Wierzbicki, M.; Pajdak, A.; Baran, P.; Zarebska, K. Isothermic heat of sorption of methane on selected hard coals. *Przemysł Chemiczny* **2019**, *98*, 625–629.
9. Pajdak, A. Parameters of N₂ and CO₂ adsorption onto coal at various temperatures. In Proceedings of the 18th International Multidisciplinary Scientific Geoconference SGEM, Albena, Bulgaria, 30 June–9 July 2018; pp. 633–640.
10. Kudasik, M.; Skoczylas, N.; Pajdak, A. The repeatability of sorption processes occurring in the coal-methane system during multiple measurement series. *Energies* **2017**, *10*, 661. [[CrossRef](#)]
11. Okolo, G.N.; Everson, R.C.; Neomagus, H.W.P.J.; Roberts, M.J.; Sakurovs, R. Comparing the porosity and surface areas of coal as measured by gas adsorption, mercury intrusion and SAXS techniques. *Fuel* **2015**, *141*, 293–304. [[CrossRef](#)]
12. Weishauptová, Z.; Sýkorová, I. Dependence of carbon dioxide sorption on the petrographic composition of bituminous coals from the Czech part of the Upper Silesian Basin, Czech Republic. *Fuel* **2011**, *90*, 312–323. [[CrossRef](#)]
13. Godyn, K.; Dutka, B. The impact of the degree of coalification on the sorption capacity of coals from the Zofiówka Monocline. *Arch. Min. Sci.* **2018**, *63*, 727–746.
14. Młynarczuk, M.; Skiba, M. The application of artificial intelligence for the identification of the maceral groups and mineral components of coal. *Comput. Geosci.* **2017**, *103*, 133–141. [[CrossRef](#)]

15. Billemont, P.; Coasne, B.; De Weireld, G. Adsorption of carbon dioxide, methane, and their mixtures in porous carbons: Effect of surface chemistry, watercontent, and pore disorder. *Langmuir* **2013**, *29*, 3328–3338. [[CrossRef](#)] [[PubMed](#)]
16. Cai, Y.; Liu, D.; Pan, Z.; Yao, Y.; Li, J.; Qiu, Y. Pore structure and its impact on CH₄ adsorption capacity and flow capability of bituminous and subbituminous coals from Northeast China. *Fuel* **2013**, *103*, 258–268. [[CrossRef](#)]
17. Pajdak, A.; Kudasik, M.; Skoczylas, N.; Wierzbicki, M.; Teixeira Palla Braga, L. Studies on the competitive sorption of CO₂ and CH₄ on hard coal. *Int. J. Greenh. Gas Control* **2019**, *90*, 102789. [[CrossRef](#)]
18. Pan, Z.J.; Connell, L. A theoretical model for gas adsorption-induced coal swelling. *Int. J. Coal Geol.* **2007**, *69*, 243–252. [[CrossRef](#)]
19. Liu, S.M.; Harpalani, S. A new theoretical approach to model sorption-induced coal shrinkage or swelling. *AAPG Bull.* **2013**, *97*, 1033–1049. [[CrossRef](#)]
20. Connell, L.; Lu, M.; Pan, Z.J. An analytical coal permeability model for tri-axial strain and stress conditions. *Int. J. Coal Geol.* **2010**, *84*, 103–114. [[CrossRef](#)]
21. Durucan, S.; Ahsanb, M.; Shia, J.-Q. Matrix shrinkage and swelling characteristics of European coals. *Energy Procedia* **2009**, *1*, 3055–3062. [[CrossRef](#)]
22. Seidle, J.P.; Huitt, L.G. Experimental Measurement of Coal Matrix Shrinkage due to Gas Emission and Implications for Cleat Matrix Increases. *SPE Pap.* **1995**, *181*, 30010.
23. Gawor, M.; Skoczylas, N. Sorption Rate of Carbon Dioxide on Coal. *Transp. Porous Media* **2014**, *101*, 269–279. [[CrossRef](#)]
24. Grabowska, K.; Sosnowski, M.; Krzywanski, J.; Sztékler, K.; Kalawa, W.; Żyłka, A.; Nowak, W. The numerical comparison of heat transfer in a coated and fixed bed of an adsorption chiller. *J. Therm. Sci.* **2018**, *27*, 421–426. [[CrossRef](#)]
25. Li, X.; Nie, B.; Zhang, R.; Chi, L. Experiment of gas diffusion and its diffusion mechanism in coal. *Int. J. Min. Sci. Technol.* **2012**, *22*, 885–889.
26. Crosdale, P.J.; Beamish, B.B.; Valix, M. Coalbed methane sorption related to coal composition. *Int. J. Coal Geol.* **1998**, *35*, 147–158. [[CrossRef](#)]
27. Harpalani, S.; Schraufnagel, R.A. Shrinkage of coal matrix with release of gas and its impact on permeability of coal. *Fuel* **1990**, *69*, 551–556. [[CrossRef](#)]
28. King, G.R.; Ertekin, T.M. A Survey of Mathematical Models Related to Methaneproduction from Coal Seams, Part 1. Empirical and Equilibrium Sorption Models. In Proceedings of the 1989 Coalbed Methane Symposium, The University of Alabama, Tuscaloosa, AL, USA, 17–20 April 1989; pp. 125–138.
29. Sercombe, J.; Vidala, R.; Galléb, C.; Adenota, F. Experimental study of gas diffusion in cement paste. *Cem. Concr. Res.* **2007**, *37*, 579–588. [[CrossRef](#)]
30. Staib, G.; Sakurovs, R.; Gray, E.M. Kinetics of coal swelling in gases: Influence of gas pressure, gas type and coal type. *Int. J. Coal Geol.* **2014**, *132*, 117–122. [[CrossRef](#)]
31. Day, S.; Fry, R.; Sakurovs, R. Swelling of coal in carbon dioxide, methane and their mixtures. *Int. J. Coal Geol.* **2012**, *93*, 40–48. [[CrossRef](#)]
32. Otake, Y.; Suuberg, E.M. Temperature dependence of solvent swelling and diffusion processes in coals. *Energy Fuels* **1997**, *11*, 1155–1164. [[CrossRef](#)]
33. Ruckenstein, E.; Vaidyanathan, A.; Youngquist, G. Sorption by solids with bidisperse pore structures. *Chem. Eng. Sci.* **1971**, *26*, 1305–1318. [[CrossRef](#)]
34. Berens, A.; Hopfenberg, H. Diffusion and relaxation in glassy polymer powders: 2. Separation of diffusion and relaxation parameters. *Polymer* **1978**, *19*, 489–496. [[CrossRef](#)]
35. King, G.; Ertekin, T.; Schwerer, F. Numerical simulation of the transient behavior of coal-seam degasification wells. *SPE Form. Eval.* **1986**, *1*, 165–183. [[CrossRef](#)]
36. Busch, A.; Gensterblum, Y.; Krooss, B.; Littke, R. Methane and carbon dioxide adsorption–diffusion experiments on coal: Upscaling and modeling. *Int. J. Coal Geol.* **2004**, *60*, 151–168. [[CrossRef](#)]
37. Staib, G.; Sakurovs, R.; Gray, E. Dispersive diffusion of gases in coals. Part I: Model development. *Fuel* **2015**, *143*, 612–619. [[CrossRef](#)]
38. Skoczylas, N.; Pajdak, A.; Kozieł, K.; Braga, L. Methane emission during gas and rock outburst on the basis of the unipore model. *Energies* **2019**, *12*, 1999.
39. Crank, J. *The Mathematics of Diffusion*; Clarendon Press: Oxford, UK, 1975.

40. Skoczylas, N.; Kudasik, M.; Topolnicki, J.; Oleszko, K.; Młynarczuk, M. Model studies on saturation of a coal sorbent with gas taking into account the geometry of spatial grains. *Przemysł Chemiczny* **2018**, *97*, 272–276.
41. Horvath, G.; Kawazoe, K. Method for the calculation of the effective pore size distribution in molecular sieve carbon. *J. Chem. Eng.* **1983**, *16*, 470–475. [[CrossRef](#)]
42. Jagiello, J.; Thommes, M. Comparison of DFT characterization methods based on N₂, Ar, CO₂, and H₂ adsorption applied to carbons with various pore size distributions. *Carbon* **2004**, *42*, 1227–1232. [[CrossRef](#)]
43. Dubinin, M.M. *Adsorpcja i Porowatość*; Wojskowa Akademia Techniczna: Warsaw, Poland, 1975.
44. Brunauer, S. *Physical Adsorption*; Princeton University Press: Princeton, NJ, USA, 1945.
45. Barrett, E.P.; Joyner, L.G.; Halenda, P.P. The determination of pore volume and area distribution in porous substances. I. Computations from nitrogen isotherms. *J. Am. Chem. Soc.* **1951**, *73*, 373–380. [[CrossRef](#)]
46. Pillalamarri, M.; Harpalani, S.; Liu, S. Gas diffusion behavior of coal and its impact on production from coalbed methane reservoirs. *Int. J. Coal Geol.* **2011**, *86*, 342–348. [[CrossRef](#)]
47. *International Classification of In-Seam Coals*; UNECE: Geneva, Switzerland; UN: New York, NY, USA, 1998; p. 41.
48. Cui, X.; Bustin, R.M.; Dipple, G. Selective transport of CO₂, CH₄ and N₂ in coals: Insights from modeling of experimental gas adsorption data. *Fuel* **2003**, *83*, 293–303. [[CrossRef](#)]
49. Airey, E.M. Gas emission from broken coal. An experimental and theoretical investigation. *Int. J. Rock Mech. Min. Sci.* **1968**, *5*, 475. [[CrossRef](#)]
50. Skoczylas, N.; Wierzbicki, M.; Murzyn, T. The influence of temperature of the coal-methane system on sorption capacity of coal, taking into account the kinetics of sorption and diffusion processes. *Prace Instytutu Mechaniki Górotworu PAN* **2013**, *15*, 75–83.



© 2019 by the authors. Licensee MDPI, Basel, Switzerland. This article is an open access article distributed under the terms and conditions of the Creative Commons Attribution (CC BY) license (<http://creativecommons.org/licenses/by/4.0/>).